Modelling Simul. Mater. Sci. Eng. **8** (2000) 25–35. Printed in the UK PII: S0965-0393(00)08126-2

Large-scale atomistic study of core structures and energetics of $\langle c + a \rangle$ $\{11\bar{2}2\}$ dislocations in hexagonal close packed metals

J R Morris†, K M Ho†, K Y Chen†, G Rengarajan‡‖ and M H Yoo§

† Ames Laboratory, US Department of Energy, Ames, IA 50011–3020, USA
‡ Department of Mechanical Engineering, Texas A & M University, College Station, TX 77843–3123, USA
§ Metals and Ceramics Division, Oak Ridge National Laboratory, Oak Ridge, TN 37831–6115, USA

Received 7 October 1998, accepted for publication 15 September 1999

Abstract. Using two different kinds of many-body potentials as well as the Lennard-Jones potential for hexagonal close packed metals, we have found that $\langle c + a \rangle$ edge dislocations with dislocation lines along $\langle 1\bar{1}00 \rangle$ can split onto the basal plane, forming a non-planar sessile structure. The 'type I' undissociated dislocation core, observed in previous papers, is shown to be stable only for small simulations. The observed dissociated core structure has a large distorted region that we interpret as a $(11\bar{2}1)$ twin nucleus, which may help the formation of $(11\bar{2}1)$ tension twins. We also find that this core structure is lower in energy than the previously observed glissile 'type II' configuration, dissociated on the $(11\bar{2}2)$ plane. The sessile splitting of the core gives rise to non-Schmid behaviour, with the twin nucleus expanding under c-axis tension, and contracting under compression.

1. Introduction

The study of dislocation core structures and the energetics associated with slip and twinning provides valuable information for the understanding of strength and ductility of materials. It is now well established that the core effects play a major role in the plastic deformation of metals [1], and could explain such behaviour as the temperature dependence of yield stress. It is also known that complex dissociations of the core significantly influence mechanical properties [2]. Atomistic simulations of dislocations are becoming viable tools to study the associated core structures, due to the increase in computational power and improvements in modelling materials at the atomistic level.

While numerous studies in the past have dealt with face centred cubic (fcc) and body centred cubic (bcc) material systems, relatively less focus has been placed on hexagonal close packed (hcp) materials. It has been known that basal slip, non-basal slip and twinning are the primary modes of plastic deformation in hcp metals (for a review, see [3]). Dislocations with a Burgers vector in the basal plane, $\boldsymbol{b} = \frac{1}{3}\langle 11\bar{2}0 \rangle$ (denoted as $\langle \boldsymbol{a} \rangle$ in this paper) may split in a manner similar to $\langle 10\bar{1} \rangle$ fcc dislocations. This dissociation may be understood by considering simple hard-sphere models. However, dislocations with non-basal Burgers vectors (e.g. $\langle \boldsymbol{c} + \boldsymbol{a} \rangle$) also significantly affect the mechanical properties of polycrystalline hcp metals, and are considerably more complicated to study than the basal slip mode [3].

‖ Current address: General Electric Corporate Research and Development, Schenectady, NY, USA.

 © 2000 IOP Publishing Ltd

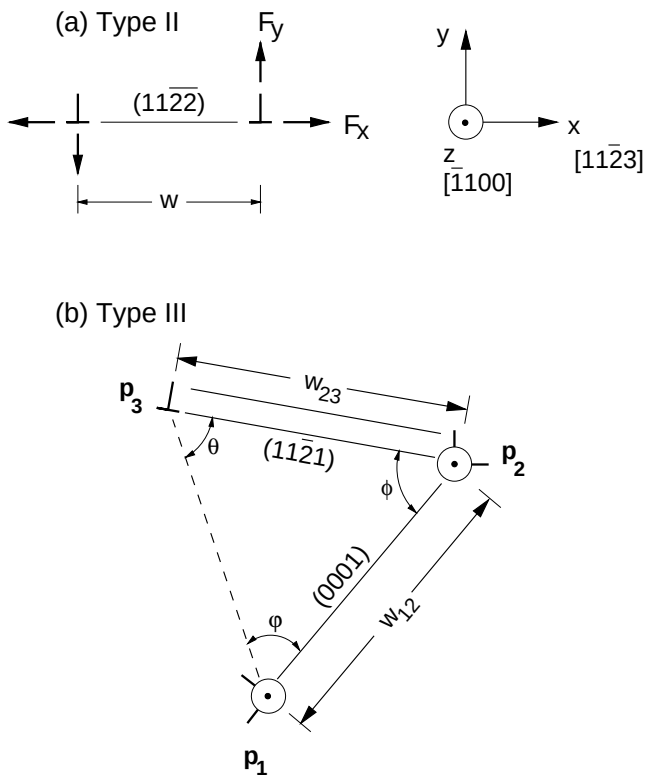

Figure 1. Schematic diagrams (*a*) and (*b*) of the type II and type III dislocation core structures, respectively. In the type III dislocation, (*b*), the dislocation has undergone a splitting into a Shockley partial $\boldsymbol{p}_1$ connected by a basal-plane stacking fault to a sessile partial $\boldsymbol{p}_2$. The twinned region extends between $\boldsymbol{p}_2$ along the (11$\bar{2}$1) plane to the twinning partials located at $\boldsymbol{p}_3$. This dissociation is given in (7). The distances and angles are given in table 3.

When a single crystal of hcp metal is deformed in compression or tension along the c-axis, plastic deformation can occur by pyramidal slip systems, e.g. [11$\bar{2}\bar{3}$]/3 slip on either the first-order (10$\bar{1}$1) or the second-order (11$\bar{2}$2) plane, and/or by compression twins including the (11$\bar{2}$2)[11$\bar{2}\bar{3}$] system or tension twin systems [3]. Because of the large magnitude of the Burgers vector, the $\langle \boldsymbol{c}+\boldsymbol{a}\rangle$ dislocation may be either decomposed to $\boldsymbol{c}$ and $\langle \boldsymbol{a}\rangle$ dislocations, or dissociated into partial dislocations that may have some relationships with the atomic movements involved in twinning. Therefore, detailed information on the source and mobility of $\langle \boldsymbol{c}+\boldsymbol{a}\rangle$ dislocations is important in understanding the mechanical behaviour of polycrystalline hcp metals and alloys.

In this paper, we re-examine previous simulations of the $\{11\bar{2}2\}\frac{1}{3}\langle 11\bar{2}\bar{3}\rangle$ edge dislocations. The previous simulations, performed by Minonishi *et al* [4, 5] and Liang and Bacon [6], produced two types of core structures: type I—an undissociated core, and type II—a dissociated core as shown in figure 1(*a*):

$$\boldsymbol{b} \longrightarrow \tfrac{1}{2}\boldsymbol{b} + \tfrac{1}{2}\boldsymbol{b}. \tag{1}$$

While this structure is expected to be lower in energy than the undissociated structure, none of the previous studies found either core to be significantly lower in energy than the other.

Our primary result is that the undissociated, 'type I' dislocation is not observed in our simulations, and that the previous simulations produced this result only due to the small size of

their simulations. An undissociated core is not observed, except in very small-size simulations. For our larger simulations, we observe either the type II core or a basal-plane dissociation after relaxation of an initially undissociated core, depending upon the initial conditions. The basal plane dissociated core, which we refer to as a type III core, is similar to that seen in recent simulations of the (Lennard-Jones) lj56 $\langle \boldsymbol{c}+\boldsymbol{a}\rangle$ edge dislocation [7]. In order to test the reliability of our results, we have used two different many-body potentials, developed for hcp metals, and also the lj56 potential used both by Minonishi [4, 5] and by Liang and Bacon [6]. In all cases, we see only the type II and type III dislocations. We believe that these two types of dislocations can account for the difference in behaviour between the brittle systems with limited twinning (Mg and Be), and ductile systems such as Ti and Zr.

2. Simulation methods and potential

As indicated above, we have used several interatomic potentials, to test the sensitivity of the results to the potentials. We believe that none of the potentials are sufficiently accurate for quantitative descriptions of the real materials and the corresponding energetics. However, structures that are potential independent are likely to represent (qualitatively) the structures that can be observed in real materials. As we shall show in subsequent sections, the observed core dissociations are independent of potential (although specific partial separations are different).

One of the potentials that we have chosen to use is the embedded atom method (EAM) potential developed by Zhang *et al* [8] (see details in [9]). This potential predicts that the hcp phase is stable relative to the fcc and bcc phases, with reasonable elastic constants and phonons for both the hcp and bcc phases. The elastic constants and other parameters are shown in table 1. This potential has been used to model the behaviour of the high-temperature bcc phase of Zr [8] and also the structure of twin boundaries in Zr [9]. More recently, it has been used to explore stacking faults on the $\{11\bar{2}2\}$ plane [10], related to the type II dislocation core structure described below. While EAM models are not ideal for modelling materials with directional bonding [11], including Ti and Zr, we feel that this model serves as a model hcp material, and may be more realistic than the simple pair potentials that have been used previously. However, it has an unphysically low basal-plane, stacking-fault energy, compared with *ab initio* potentials (see table 2).

Table 1. Equilibrium values calculated for EAM and FS models of hcp Zr, compared with experimental values.

Parameter	EAM [10]	FS [13]	Experiment	Reference
E_{coh} (eV)	6.253 79	6.25	6.25	Brewer [25]
a (Å)	3.21	3.25	3.23	Goldak *et al* [26]
c/a	1.63	1.595	1.592	Goldak *et al* [26]
C_{11} (Mbar)	1.63	1.5	1.554	Fisher and Renken [27]
C_{12} (Mbar)	0.93	0.85	0.672	
C_{13} (Mbar)	0.78	0.67	0.646	
C_{33} (Mbar)	1.78	1.75	1.725	
C_{44} (Mbar)	0.27	0.36	0.363	

Recognizing that a single potential may have unphysical aspects, it is important to identify which results are dependent upon the potential, and which are independent of the potential. To this end, we have also used a Finnis–Sinclair (FS) potential [12] for Zr developed by Ackland *et al* [13]. These potentials are similar to the EAM model, with the same drawbacks. This particular potential more accurately reproduces the experimental c/a ratio than the Zr EAM

Table 2. Basal-plane, stacking-fault energies and $\boldsymbol{p}_1$–$\boldsymbol{p}_2$ separations from atomistic simulations and from estimations from linear anisotropic elastic theory. Separations are given in units of the lattice spacing a_0. For comparison, *ab initio* calculations of stacking-fault energies for Mg [19] and Zr [20] have been included.

				ab initio	
	Zr EAM	Zr FS	lj56	Zr	Mg
Stacking-fault energy (mJ m^{-2})	3.3	50	0.138	102	44
Simulated $\boldsymbol{p}_1$–$\boldsymbol{p}_2$ separation (a_0)	12	5	5	—	—
Estimated $\boldsymbol{p}_1$–$\boldsymbol{p}_2$ separation (a_0)	167	12	—	5.9	5.3

potential described above. It also has a significantly higher (and more accurate) basal-plane, stacking-fault, energy. Most of the figures in this paper were generated using this potential.

In addition, we have also repeated some of the calculations using the lj56 potential [14]. This was chosen primarily to compare with the results of Minonishi *et al* [4, 5] and Liang and Bacon [15] who performed simulations of the same dislocation considered here using the lj56 potential. Previous work differs from ours primarily in the size of the simulation. As we shall show below, this directly affects the observed dislocation core structures.

The initial conditions were generated as in previous studies [4, 6]. A displacement field was calculated from anisotropic elasticity [16, 17], corresponding to a perfect dislocation with a Burgers vector $\boldsymbol{b} = \langle \boldsymbol{c} + \boldsymbol{a} \rangle$. This displacement field was imposed on a perfect lattice, with a number of different starting positions of the dislocation. From this structure, a cylindrical region was chosen, including all atoms within a distance R of the dislocation line. In all of these studies, we set R to either 120 Å or 180 Å, to check the effects of the system size. No differences were found between these different simulation sizes. The repeat distance along the line of the dislocation was chosen to be four times $[1\bar{1}00]$. Thus, the simulation is essentially two dimensional.

Once this region was selected, an outer 'frozen zone' was selected. In this outer zone, the atoms were fixed during the simulations. This zone was chosen to be all of the atoms within 10 Å from the outer surface of the simulation, somewhat larger than the interaction distance for the EAM or FS potentials. The size of the simulation region plays an important role in determining the core structure. As shown later, a small simulation region can prevent the core from splitting, and hence, may produce a stable undissociated core. In comparable simulations, Minonishi *et al* [5] used a total of approximately 8000 atoms, and Liang and Bacon [6] used a total of 9000 atoms. However, the number of atoms in the inner 'relaxable' region was about 1000 in both papers, which may not be large enough to give the splitting of dislocations. In order to overcome this limitation, we have performed large-scale simulations, using approximately 97 000 atoms, of which about 86 000 atoms are free to relax, and have thus minimized the size effects.

For the lj56 potential, we chose a rectangular box shape, with an active region ranging from $-40d$ to $40d$ in the x-direction (along the Burgers vector) and from $-35d$ to $35d$ in the y-direction. This left a total of 50 000 atoms free to move. We chose this size to explore size effects (see discussion), in order to compare with the lj56 simulations of Minonishi *et al* [4, 5].

After generating the initial coordinates, we used a classical molecular dynamics (MD) code to perform a rapid quench of the system, in order to find a local minimum in the energy. This was performed using the 'dynamic' technique [18]. For the EAM model, the atomic relaxation was also carried out independently using a simple steepest-descent technique, producing nearly identical results. Following this, we performed MD simulations of the system at $T = 500$ K for

approximately 40 ps, in order to 'anneal' the structure. Finally, another quench was performed. In all cases, the dislocation structure after the final quench was qualitatively the same as after the initial quench. Based upon these results, we only used the dynamic technique for atomic relaxation, for the FS and the lj56 systems.

3. Non-planar dislocation core structures

To fully explore the possible dislocation structures, we tried a series of 12 initial conditions. For each potential, we found that certain initial conditions resulted in structures corresponding to a type II dislocation observed in previous simulations [4, 6]. In the remaining cases, a new structure, which we have denoted as a type III dissociation, was observed. We did not observe an undissociated (type I) structure after the initial quench. We note that there did not seem to be any correlation between the initial conditions that produced the type III dislocations in one potential, and those that produced these configurations in other potentials.

As the type II structure has been thoroughly studied [4, 6], we will only describe the type III structure. The core structure for the FS potential is shown in figure 2. The most interesting feature is a large distorted region extending to the left and upwards from the dislocation. This contains a small area that is twinned on the $(11\bar{2}1)$ planes, as indicated by the traces on the figure. This is very similar to the twinned regions near type I cores seen in [4, 6]. However, there is an important difference: the dislocation dissociates according to

$$\boldsymbol{b} \rightarrow \tfrac{1}{3}[10\bar{1}0] + \tfrac{1}{3}[01\bar{1}\bar{3}] \tag{2}$$

with the first of these terminating a basal-plane stacking fault. This non-planar splitting is a sessile configuration, unlikely to slip on the $(11\bar{2}2)$ plane.

We will denote this dissociation by

$$\boldsymbol{b} \rightarrow \boldsymbol{p}_1 + \boldsymbol{p}_2 \tag{3}$$

with the identification

$$\boldsymbol{p}_1 \equiv \tfrac{1}{3}[10\bar{1}0] \tag{4}$$

$$\boldsymbol{p}_2 \equiv \tfrac{1}{3}[01\bar{1}\bar{3}]. \tag{5}$$

The partial $\boldsymbol{p}_1$ also occurs in the usual splitting of the $\langle \boldsymbol{a}\rangle$ Burgers vector,

$$\tfrac{1}{3}[11\bar{2}0] \rightarrow \tfrac{1}{3}[10\bar{1}0] + \tfrac{1}{3}[01\bar{1}0]. \tag{6}$$

To identify the partial $\boldsymbol{p}_1$, we examined the relative displacements around the dislocation. In figure 3, the relative displacement of the basal planes immediately above and below the partial $\boldsymbol{p}_1$ is shown. There are relative motions both parallel and perpendicular to the line, indicating the mixed nature of the $\boldsymbol{p}_1$ partial dislocation. The edge component is dominant, with the magnitude of the screw component smaller by a factor of $\sqrt{3}$. This indicates that the Burgers vector is at an angle of 60° to the line of the dislocation. This, combined with the calculated total magnitude of the Burgers vector, is consistent with the dissociation given in (2).

The separation of the partials along the basal plane (equation (2)) is significant, approximately 22 Å for the FS potential. The separations for each potential are given in table 2. From this table, we see that there is a correlation between the basal-plane, stacking-fault energies and the separation: a larger value of the stacking-fault energy reduces the separation. However, the separation is significantly less than what would be predicted from anisotropic linear elasticity theory, based upon (2).

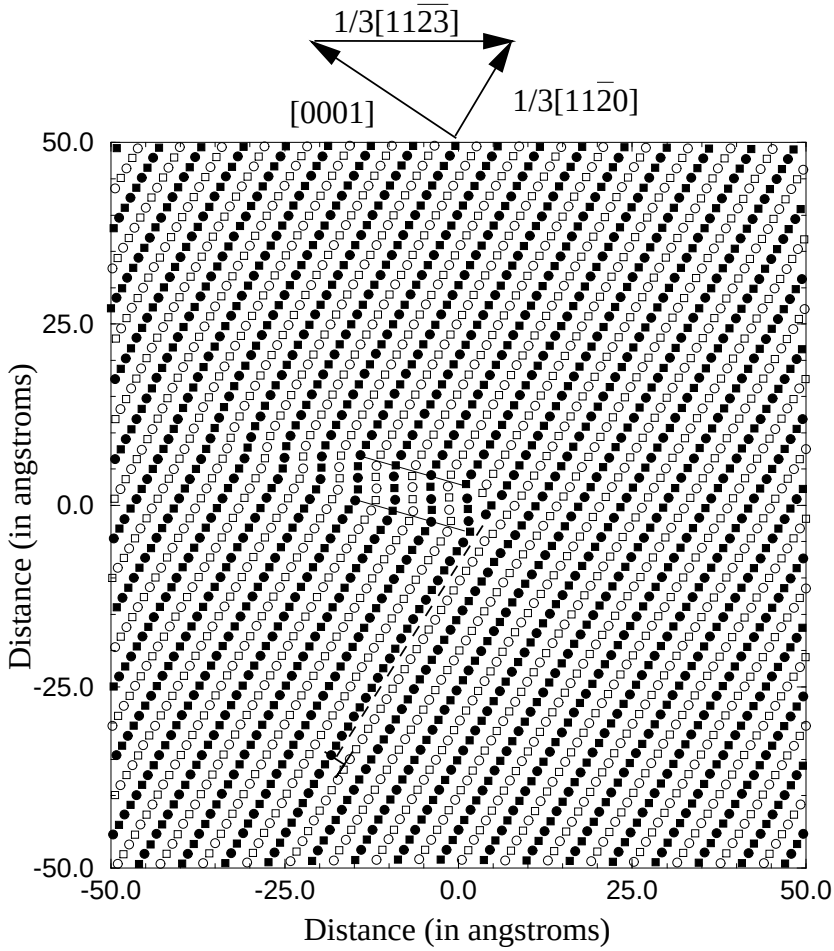

Figure 2. The structure of the type III dislocation. The dislocation has split according to $b \rightarrow \frac{1}{3}[10\bar{1}0] + \frac{1}{3}[01\bar{1}3]$, with the partials separated by a basal-plane stacking fault.

Type III dissociations found for the EAM and lj56 potentials were similar. The separations for both the FS and EAM potentials are shown in table 3, along with the stacking-fault energy for each potential. The stacking-fault energy is particularly low for the EAM potential, producing the largest splitting. To provide a comparison, we note that the *ab initio* calculations of the stacking-fault energy for Mg is 44 mJ m^{-2} [19] and 102 mJ m^{-2} for Zr [20]. Bond-order potential calculations for Ti produce stacking-fault energies similar to the *ab initio* Zr results [11]. Although the empirical potentials generally produce lower stacking-fault energies than the more accurate *ab initio* results, the separation is significant in all cases.

Table 3 shows a qualitative correlation between the basal-plane, stacking-fault energy Γ_{b} and the $\boldsymbol{p}_1 - \boldsymbol{p}_2$ splitting w_{12}. Including only the interaction between the $\boldsymbol{p}_1$ and $\boldsymbol{p}_2$ dislocations is overly simplistic for the type III dislocation core, because there are additional interactions with the twin nucleus. While difficult to account for in an accurate manner, we present a schematic approach in figure 1(*b*). In this figure, we have added twinning dislocations at either side of the twin nucleus, sufficient to produce a four-layer twin. For the $\frac{1}{3}(11\bar{2}1)[\bar{1}\bar{1}26]$ tension twin system, twinning partials have Burgers vectors of $\boldsymbol{b}_{\mathrm{t}} = (e/2)\eta$, where $\eta = \frac{1}{3}[\bar{1}\bar{1}26]$ and

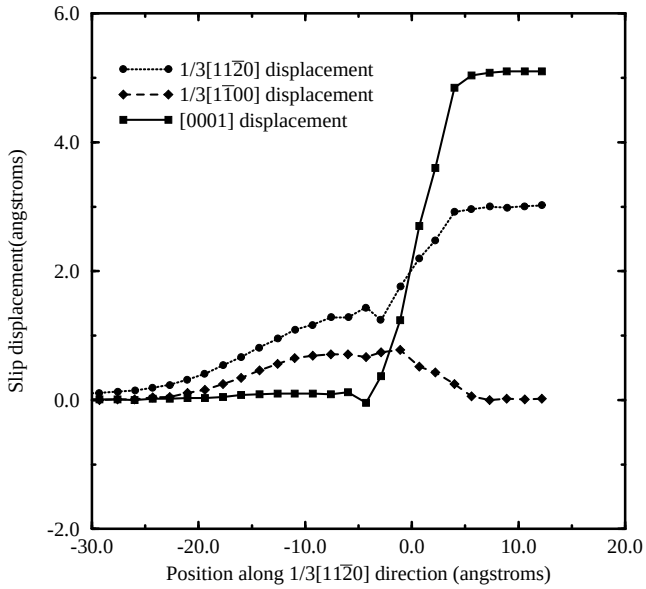

Figure 3. This figure shows the relative displacement of (0001) basal planes passing around the dislocation in the type III dissociation. From this figure, we see that the partial $\boldsymbol{p}_1$ has both a $[11\bar{2}0]$ edge components, and a $[1\bar{1}00]$ screw component. The Burgers vector of the partial $\boldsymbol{p}_1$ forms an angle of 60° with the line of the dislocation.

Table 3. Geometry of the type III dislocation core dissociations, along with basal-plane, stacking-fault energies and $(11\bar{2}1)$ twin boundary energies derived from the separations. The widths w_{12} and w_{23} are the $\boldsymbol{p}_1$–$\boldsymbol{p}_2$ separation and the twin nucleus width, respectively. For definitions of θ and ϕ, see figure 1(*b*).

	w_{12} (nm)	w_{23} (nm)	ϕ (degrees)	θ (degrees)	Γ (mJ m^{-2}) (0001)	Γ (mJ m^{-2}) $(11\bar{2}1)$
EAM	4.2	3.6	50.6	56.5	26	99
FS	2.2	4.2	76.4	30.7	140	47

$e = 2/(4\gamma^2+1) \approx \frac{1}{6}$ for Zr with $\gamma \equiv c/a = 1.63$ [21]. Therefore, the total strength of four twinning partials is $\boldsymbol{p}_3 = [\bar{1}\bar{1}26]/9$. Consequently, the Burgers vector of the sessile partial located at the corner of this non-planar dissociation is $\boldsymbol{p}_2 = [14\bar{5}3]/9$. Thus, the splitting given in (2) has been modified to

$$\boldsymbol{b} \rightarrow \tfrac{1}{3}[10\bar{1}0] + \tfrac{1}{9}[14\bar{5}3] + \tfrac{1}{9}[\bar{1}\bar{1}26]. \tag{7}$$

The widths of the basal stacking fault, w_{12}, and the tension twin, w_{23}, are given in table 3. The angle between the twin habit plane and the basal plane is $\Phi = \tan^{-1}(2\gamma) = 73.0°$. The other two angles, θ and ϕ, defined in figure 1(*b*) are also given in table 3. Using anisotropic elasticity theory, we calculated the forces on the dislocations. Both F_x and F_y force components (along the $\langle \boldsymbol{c}+\boldsymbol{a}\rangle$ direction and perpendicular to the $(11\bar{2}2)$ plane, respectively) of the pair-wise interaction were calculated first. The net results of F_x in the fault planes were determined at $\boldsymbol{p}_1$ and $\boldsymbol{p}_3$. By requiring that the total glide forces balance to zero, we calculate the basal-plane, stacking-fault energy, Γ_{b}, and twice the $(11\bar{2}1)$ twin boundary energy, $2\Gamma_{\mathrm{t}}$. These results with the two sets of elastic constants are listed in table 3.

As compared to $\Gamma_b = 3.3$ mJ m^{-2} and $\Gamma_t = 285$ mJ m^{-2} [22] calculated using the EAM potential, the basal-plane, stacking-fault energy is higher by a factor of 7.9, while the twin boundary energy is lower by a factor of 5.8. Based upon the FS potential, we obtain $\Gamma_b = 50$ mJ m^{-2}, and Serra and Bacon [23] reported $\Gamma_t = 278$ mJ m^{-2}. As compared to these results for Γ_b and Γ_t, the values listed in table 3 are higher by a factor of 2.8 and lower by a factor of 11.8, respectively. This comparison suggests that nonlinear elastic interactions, ignored in this analysis, assist in the twin nucleation, creating a larger than expected twinned region. Simultaneously, the complementary splitting on the basal plane is suppressed.

We note that we have not observed a separation into separate $\boldsymbol{c}$ and $\langle \boldsymbol{a} \rangle$ dislocations. Within isotropic, linear elasticity theory, there should be no reason for these to interact, and we would expect that they could separate. However, this neglects two points. First, anisotropy can introduce an interaction between these dislocations. However, this can be expected to be weak. Second, they may lower their energy through an interaction of the dislocation cores. This effect is beyond the assumptions of linear elasticity theory. We have applied a strain on the basal plane, coupling to the $\langle \boldsymbol{a} \rangle$ portion of the dislocation, to attempt to separate the dislocations. We find that under reasonably strong strains (2%), this has the effect of increasing the $\langle \boldsymbol{p}_1 \rangle$ partial separation, without unbinding the dislocations.

4. Energy calculations

Given that several possible dislocation structures exist, it is important to consider the energy of the dislocations. While the energy of a single dislocation in an infinite crystal is not defined, we may compare the core energies of different core structures, to find which structure has the lowest energy.

To do this, we consider the energy contained within a distance R from the dislocation. The total energy E_T per unit length of the dislocation in the region defined by $(0, R)$ may be written as

$$E_T = E_c(r_c) + E_e(r_c, R) \tag{8}$$

where $E_c(r_c)$ is the energy in the 'core' region, where linear elasticity is not applicable. (Note that the choice of r_c also defines the value of E_c.) The elastic energy outside the core region, $E_e(r_c, R)$, is given by [24]

$$E_e = \frac{K_e}{4\pi} b^2 \ln \frac{R}{r_c} \tag{9}$$

where K_e is the energy factor determined from anisotropic elasticity theory. From the geometry of the $\langle \boldsymbol{c} + \boldsymbol{a} \rangle$ dislocation and the elastic constants given in table 1, we find the value $K_e = 0.385$ eV Å^{-3} for the FS potential.

We may also calculate the energy from the distortions of the dislocation from atomistic simulations. If the equilibrium bulk energy per atom in the pure hcp structure is E_0, then the excess energy due to the atomic displacements within a distance R of the dislocation core is

$$E_T = \frac{1}{d} \sum_i (E_i - E_0) \tag{10}$$

where E_i is the total potential energy of atom i, d is the repeat distance along the direction of the dislocation line (for this geometry, $d = \sqrt{3}a_0$) and the sum extends for atoms within a distance R of the dislocation core. At long distances, the behaviour should follow that of (9).

Figure 4 shows the variation of calculated elastic energies with the logarithm of the radius from the core, from the results for the FS potential. From this, we see that the basal plane splitting (type III) is significantly lower in energy than that of the type II dislocation.

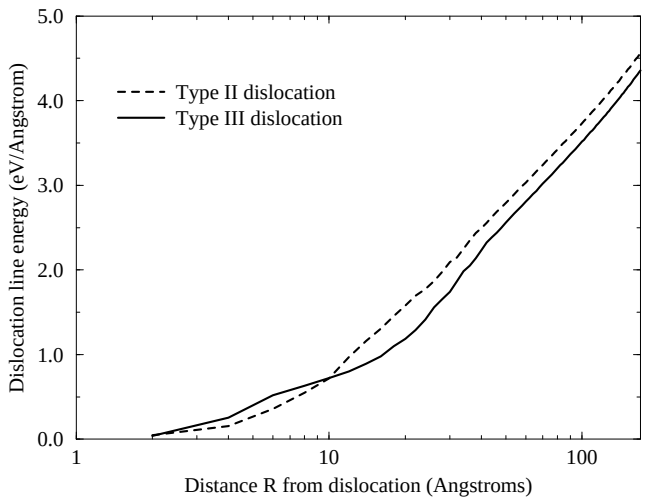

Figure 4. Energy $E_{\mathrm{T}}(R)$ per unit length of the dislocation, for the two types of dislocation found in the simulations, as a function of R. The dislocation energy is given in units of eV Å^{-1}.

A similar calculation for both EAM and the lj56 potentials again shows that the type III dislocation is lower in energy. At large distances (greater than approximately 40 Å), the graphs are essentially parallel. This indicates that for $R > 40$ Å, the energies found in the simulations behave as predicted by elasticity theory. At large distances, the energy difference between the two structures corresponds to the difference in the total energy of the dislocations.

5. Discussion

In this paper, we have used atomistic simulations to explore possible core structures of the $\langle \boldsymbol{c}+\boldsymbol{a}\rangle$ edge dislocation. We expect that this dislocation core plays an important (and complicated) role in determining the behaviour of hcp metals under c-axis compression and tension. For Mg and Be, the dominant deformation mode is the $(11\bar{2}2)$ $\langle \boldsymbol{c}+\boldsymbol{a}\rangle$ slip system; the compression twinning mode in Ti and Zr has the same elements. Therefore, it is expected that $\langle \boldsymbol{c}+\boldsymbol{a}\rangle$ dislocations may determine the non-basal deformation mode.

Our simulation techniques are similar to those performed by Minonishi *et al* [4, 5] and by Liang and Bacon [6]. However, they differ in several respects. First, in addition to simple pair potentials, we have also used more sophisticated EAM and FS potentials fitted to equilibrium properties. Second, and most importantly, we have used significantly larger system sizes. Finally, we have not only performed local minimization, but we have also annealed the dislocation cores in an effort to find the lowest-energy structures.

Unlike previous investigations [4–6] we do not observe a stable, undissociated core. Instead, we see a new core dissociation, which we label as 'type III', where the core emits a $\boldsymbol{p}_1 \equiv \frac{1}{3}[10\bar{1}0]$ partial dislocation along the basal plane. The remaining partial has a core structure containing a $(11\bar{2}1)$ twin nucleus, similar to the undissociated 'type I' core found in previous simulations [4–6]. We observe the type II dislocation found previously [5, 6], in which the dislocation splits along the $(11\bar{2}2)$ slip plane, with a stable stacking fault on the slip plane. We have found that the type III dislocation has a core energy that is lower than that of the type II, by analysing the energy distribution in our simulations.

We believe that previous simulations [4–6] were severely affected by the small system sizes. In these previous simulations, only a small region (about 1000 atoms) is allowed to relax. This prevented the type III core from forming. Having only a small region to dissociate, and having to match the boundary conditions, prevents the partial $\boldsymbol{p}_1$ from separating from the original dislocation. We have tested size effects for the type III dislocation for the EAM, FS and lj56 potentials. For these calculations, we chose a rectangular system, and varied the size of the system. For the EAM potential, which has a large splitting, the system size must be made very small ($\sim$15 Å normal to the $(11\bar{2}2)$ plane) in order to suppress the dissociation. For the FS and lj56 systems, however, the splitting for the large system is still not too large, and is suppressed rather easily. Once the system size perpendicular to the $(11\bar{2}2)$ plane is smaller than $\sim 15a_0$, then the core remains in an undissociated (type I) configuration.

The splittings are very sensitive to the stacking-fault energy, and are not likely to be accurately modelled for any given material by any of these potentials. In particular, Zr and Ti have large basal-plane, stacking-fault energies, close to 100 mJ m^{-2} [11, 20]. Basal-plane slip is therefore not usually observed in these materials. However, the stacking fault is stable [11, 20], and so a type III dissociation may occur for these materials.

We expect that the type III core will be more sessile than the type II, as the partials for the latter core will slip on the $(11\bar{2}2)$ plane. For the type III core, the partial $\boldsymbol{p}_1$ moves on the basal plane, while the $\boldsymbol{p}_2$ partial should slip on the $(11\bar{2}1)$ plane. Thus, the two partials cannot move together. We also expect that shear on the $(11\bar{2}2)$ plane will have a different effect on the type III dislocation than compression/tension along the c-axis, as the latter will not couple to the motion of the $\boldsymbol{p}_1$ partial along its easy-slip direction.

It is possible that different types of cores occur in different materials, giving rise to different behaviour under c-axis compression and tension. It is plausible that in a material where the dislocation has a type II structure, that the $(11\bar{2}2)$ slip will be the deformation mode. If the type III structure occurs, then the lack of mobility may hinder slip, and twinning may be favoured. We also note that the presence of a type III configuration may assist in the nucleation of $(11\bar{2}1)$ twins. This suggests that there may be a correlation between metals that exhibit compression twinning on the $(11\bar{2}2)$ plane, and those that have tension twinning on the $(11\bar{2}1)$ plane. This is borne out by experiments: Ti and Zr show both types of twin modes, while Be and Mg show neither [3].

In conclusion, we have observed two different core structures for the $\langle \boldsymbol{c} + \boldsymbol{a} \rangle$ edge dislocation in simulations of hcp materials. Both of these structures are dissociated, with the type III structure (not observed in previous simulations) having a sessile geometry, splitting along the basal plane. For all potentials considered here, this latter type is lower in energy.

Acknowledgments

This research used resources of the Center for Computational Sciences at Oak Ridge National Laboratory (ORNL) and the Scalable Computing Laboratory, funded by Iowa State University and Ames Laboratory. This work was supported by the High Performance Computing and Communications Initiative (HPCCI). Ames Laboratory is operated for the US Department of Energy by Iowa State University under contract no W-7405-Eng-82. The work at ORNL was sponsored by the Division of Materials Sciences, Office of Basic Energy Sciences, US Department of Energy under contract no DE-AC05-96OR22464 with Lockheed Martin Energy Research Corporation.

References

[1] Vitek V 1992 *Prog. Mater. Sci.* **36** 1
[2] Duesbery M S 1997 *Dislocations in Solids* vol 10, ed F R N Nabarro (Amsterdam: North-Holland) p 67
[3] Yoo M H 1981 *Metall. Trans.* A **12** 409
[4] Minonishi Y, Ishioka S, Koiwa M, Morozumi S and Yamaguchi M 1981 *Phil. Mag.* A **44** 1225
[5] Minonishi Y, Ishioka S, Koiwa M, Morozumi S and Yamaguchi M 1982 *Phil. Mag.* A **45** 835
[6] Liang M H and Bacon D J 1986 *Phil. Mag.* A **53** 181
[7] Ando S, Takashima K and Tonda H 1996 *Mater. Trans. Japan. Inst. Metals* **37** 319
[8] Zhang B L, Wang C Z, Ho K M, Turner D E and Ye Y Y 1995 *Phys. Rev. Lett.* **74** 1375
[9] Morris J R, Ye Y Y, Ho K M, Chan C T and Yoo M H 1995 *Phil. Mag.* A **72** 751
[10] Morris J R, Scharff J, Ho K M, Ye Y Y and Yoo M H 1997 *Phil. Mag.* A **76** 1065
[11] Girshick A, Pettifor D G and Vitek V 1998 *Phil. Mag.* A **77** 999
[12] Finnis M W and Sinclair J E 1984 *Phil. Mag.* A **50** 45
[13] Ackland G J, Wooding S J and Bacon D J 1995 *Phil. Mag.* A **71** 553
[14] Bacon D J and Martin J W 1981 *Phil. Mag.* A **43** 883
[15] Liang M H and Bacon D J 1986 *Phil. Mag.* A **53** 205
[16] Yoo M H and Loh B T M 1970 *J. Appl. Phys.* **41** 2805
[17] Stroh A N 1958 *Phil. Mag.* A **3** 625
[18] Gehlen P C 1970 *J. Appl. Phys.* **41** 5165
[19] Chetty N and Weinert M 1997 *Phys. Rev.* B **56** 10 844
[20] Morris J R and Ye Y Y 1999 in preparation
[21] Yoo M H 1969 *Trans. AIME* **245** 2051
[22] Morris J R, Ye Y Y, Ho K M, Chan C T and Yoo M H 1994 *Twinning in Advanced Materials* ed M H Yoo and M Wuttig (Warrendale, PA: Minerals, Metals and Materials Society) p 43
[23] Serra A and Bacon D J 1993 *Mater. Sci. Forum* **126–128** 69
[24] Hirth J P and Lothe J 1968 *Theory of Dislocations* (New York: McGraw-Hill)
[25] Brewer L 1975 *Lawrence Berkeley Laboratory, Report No 3720* unpublished
[26] Goldak J, Lloyd L T and Barrett C S 1966 *Phys. Rev.* **144** 474
[27] Fisher E S and Renken C J 1964 *Phys. Rev.* A **135** A482